The Effect of Transformation Induced Plasticity on the Mechanical Behavior of Porous SMAs

Dimitris C. Lagoudas[a], Pavlin B. Entchev[a] and Eric L. Vandygriff[a]

[a] Center for Mechanics of Composites, Aerospace Engineering Department
Texas A&M University, College Station, TX 77843-3141

ABSTRACT

The fabrication of porous NiTi Shape Memory Alloy (SMA) from elemental Ni and Ti powders using Hot Isostatic Press (HIP) is presented in this work. Porous NiTi alloys with different porosity levels and different mechanical properties are obtained and analyzed. Their behavior under compressive mechanical loading is modeled using a micromechanical averaging model. The model treats the porous NiTi alloy as a two-phase composite: dense SMA matrix and pores. The behavior of the fully dense SMA matrix is modeled using a thermomechanical model with internal state variables. The development of transformation and plastic strains during the martensitic phase transformation is taken into account. The results from the model are compared with the experimental data.

Keywords: Porous Shape Memory Alloy, NiTi, Powder Metallurgy, Micromechanics, Mori-Tanaka

1. INTRODUCTION

Shape Memory Alloys (SMAs) are metallic alloys which can recover permanent strains when they are heated above a certain temperature. The key characteristic of all SMAs is the occurrence of a martensitic phase transformation. The martensitic transformation is a shear-dominant diffusionless solid-state phase transformation occurring by nucleation and growth of the martensitic phase from a parent austenitic phase.

Due to their unique properties, SMAs have attracted great interest in various fields of applications ranging from aerospace[1,2] and naval[3] to surgical instruments[4] and medical implants and fixtures.[5,6] The SMAs have been used in coupling devices,[7] as actuators in a wide range of applications[8] as well as in medicine and dentistry.[9] These applications have mostly benefited from the ability of the inherent shape recovery characteristics of SMAs. In addition to the shape memory and pseudoelasticity effects that SMAs possess, there is also the promise of using SMAs in making high-efficiency damping devices that are superior to those made of conventional materials, partially due to their hysteretic response.

Driven by biomedical applications, recent emphasis has been given to *porous SMAs*. The possibility of producing SMAs in porous form opens new fields of application, including reduced weight and increased biocompatibility. Perhaps the most successful application of porous SMAs to this date is their use as bone implants.[10–12] One of the main reasons for such a success is the biocompatibility of the NiTi alloys used in the above cited works. In addition, the porous structure of the alloys allows ingrowth of the tissue into the implant.

In the last several years since the fabrication techniques for porous SMAs have been established, additional applications have also been considered. The potential applications of porous SMAs will utilize their ability to carry significant loads. Beyond the energy absorption capability of dense SMA materials, porous SMAs offer the possibility of higher specific damping capacity under dynamic loading conditions. One of the applications, which utilizes the energy absorption capabilities of the porous SMAs, is the development of effective dampers and shock absorbing devices. It has been demonstrated that a significant part of the impact energy is absorbed.[13] The reason for such high energy absorption is the sequence of forward and reverse phase transformations in the

Further author information:
D.C.L.: E-mail: lagoudas@aero.tamu.edu, Telephone: 1 979 845 1604 (Corresponding author)
P.B.E.: E-mail: pavlin@aero.tamu.edu, Telephone: 1 979 845 0716
E.L.V.: E-mail: evandygriff@tamu.edu, Telephone: 1 979 845 5290

SMA matrix. In addition to the inherent energy dissipation capabilities of the SMA matrix, it is envisioned that the pores will facilitate additional absorption of the impact energy due to wave scattering.

Another advantage of the porous SMAs over their fully dense counterparts is the possibility to fabricate them with gradient porosity. This porosity gradient offers enormous advantage in applications involving impedance matching at connecting joints and across interfaces between materials with dissimilar mechanical properties. The use of such porous SMA connecting elements will prevent failure due to wave reflections at the interfaces, while at the same time providing the connecting joint with energy absorption capabilities. Also, currently of great interest is the use of porous SMAs in various vibration isolation devices. It is envisioned that such devices will find applications in various fields ranging from isolation of machines and equipment to isolation of payloads during launch of space vehicles. To increase the energy absorption capabilities a second phase, which would fill the pores, can be added. It should be noted that these latest developments are still being actively researched and have not yet been used in commercial applications.

Different fabrication techniques for producing porous SMAs have been established. While some of the works focus on fabrication of porous SMAs by injecting a gas into a melt,[14] most of the research work on fabrication of porous SMAs has focused on using powder metallurgy techniques.[15–21] Different fabrication techniques for producing porous SMAs from elemental powders have been used. Some of the difficulties that may be encountered with the use of elemental powders include contamination from oxides and the formation of other intermetallic phases. On the other hand, producing pre-alloyed NiTi powder requires processing techniques which are both difficult and expensive due to the hardness of the alloy.

Techniques that are currently being used to produce porous NiTi from elemental powders include self-propagating high-temperature synthesis, conventional sintering, and sintering at elevated pressures via a Hot Isostatic Press (HIP). Some advantages of sintering at elevated pressure include shorter heating times than conventional sintering and the ability to produce near net shape objects that require less time to machine. The current work uses porous NiTi fabricated using the HIPping technique.[20] Two different porous NiTi alloys were obtained: at lower fabrication temperature (900°C) a porous material with smaller pore sizes is obtained, while for higher temperature (950°C) the sizes of the pores are significantly larger.

In previous works the behavior of porous SMAs under compressive mechanical loading has been modeled using an incremental formulation of the Mori-Tanaka method.[22–24] The porous material has been modeled as a composite with fully dense SMA matrix and pores. The behavior of the SMA matrix have been modeled using the constitutive model presented by Lagoudas et al.[25] In the current work the constitutive model for the dense SMA matrix is modified to take into account the development of plastic strains during the martensitic phase transformation.

The remainder of the paper is organized as follows: the next section is separated into two parts; first, the fabrication process for HIPped porous SMAs will be briefly described, then characterization of the material is presented as experimental results including micrographs, calorimetric measurements, and quasi-static testing under compressive loads. Section 3 describes the modeling of porous NiTi SMA with subsections on the micromechanical modeling, constitutive modeling of the dense SMA matrix and the evaluation of the material parameters. Modeling results are presented in Section 4. Finally, conclusions are made in Section 5.

2. MECHANICAL PROPERTIES OF POROUS SMAS FABRICATED VIA A HOT ISOSTATIC PRESS

2.1. Fabrication of Porous NiTi SMA

Porous NiTi specimens were fabricated from elemental Ni and Ti powders using HIPping technique in the Active Materials Laboratory at Texas A&M University.[20] Using two slightly different processing cycles, two different porous NiTi alloys were produced. The first alloy was fabricated at a temperature of 900°C and is characterized by its small pore size (on the order of 25 μm). The fabrication temperature for the second alloy was 950°C and the sizes of its pores are significantly larger (pores as large as 1 mm are observed). A detailed analysis of the composition of the two alloys was performed by Lagoudas and Vandygriff[26] using Energy-Dispersive X-ray Spectrometry (EDS) and further using Wave-Dispersive X-ray Spectrometry (WDS). The analysis has

revealed evidence of multiple intermetallic phases present in both large and small pore alloys. The greater part of the material for large pore alloys was identified as equiatomic NiTi. However, the material contains numerous needle-like structures having a width of approximately one-half micron. These needle-like structures were too small to be analyzed without interference from the surrounding medium. By analyzing some of the larger intersections of needle phases however, it is presumed by a slight increase in the percentage of Ni that the needle phases are Ni rich phases. For the small pore alloy five different phases, i.e., NiTi, Ni_2Ti, $NiTi_3$ and elemental Ni and Ti were identified. The apparent reason for the presence of relatively large intermetallic phase regions in the small pore alloy is the lower fabrication temperature, which leads to incomplete diffusion of the elemental powders.

The porosity of the specimens was measured by taking micrographs and estimating the ratio of the area occupied by the pores to the total area at different cross-sections. The estimate of the porosity was also verified by comparing the density of the porous NiTi material with the theoretical density of fully dense NiTi. The porosity of the small pore alloy is estimated to be equal to 50% while the porosity of the large pore alloy is equal to 42%. Micrographs of typical specimens for both small and large pore alloys are shown in Figure 1. The dark areas on the micrographs, shown in Figure 1 represent the pores, while the lighter areas are occupied by NiTi.

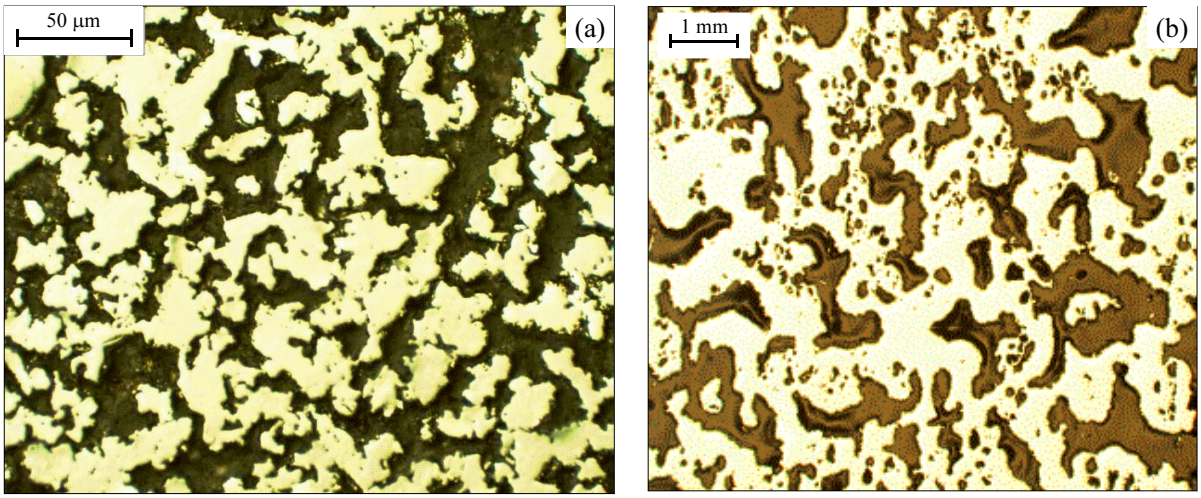

Figure 1: Microphotograph of porous NiTi specimens: (a) small pore specimen; (b) large pore specimen.

The porous NiTi specimens were further analyzed using differential calorimetry techniques. The DSC test curves for both small and large pore alloys are shown in Figure 2. The upper curves seen in Figure 2 represent the normalized heat flow into the specimen during heating and the lower curves represent the heat flow out of the specimen upon cooling. The tests indicate solid-solid phase transformation at approximately 44°C and 42°C for the small and large pore alloys during heating (martensite-to-austenite) and −12°C and 20°C during cooling (austenite-to-martensite) for the small and large pore specimens, respectively. Therefore, depending on whether the specimen was previously heated or cooled, either martensite or austenite crystalline structure can be present at room temperature (22°C). The cooling curves for both alloys show evidence of a dual peak that is indicative of an R-phase.

2.2. Mechanical Properties of HIPped Porous NiTi

Next, the HIPped porous NiTi specimens were mechanically tested under quasi-static compressive loads. For testing, the fabricated porous NiTi specimens were machined to cylindrical shapes with a nominal diameter of 13 mm and a length of 35 mm. After the fabrication of the porous specimens they have not been subjected to

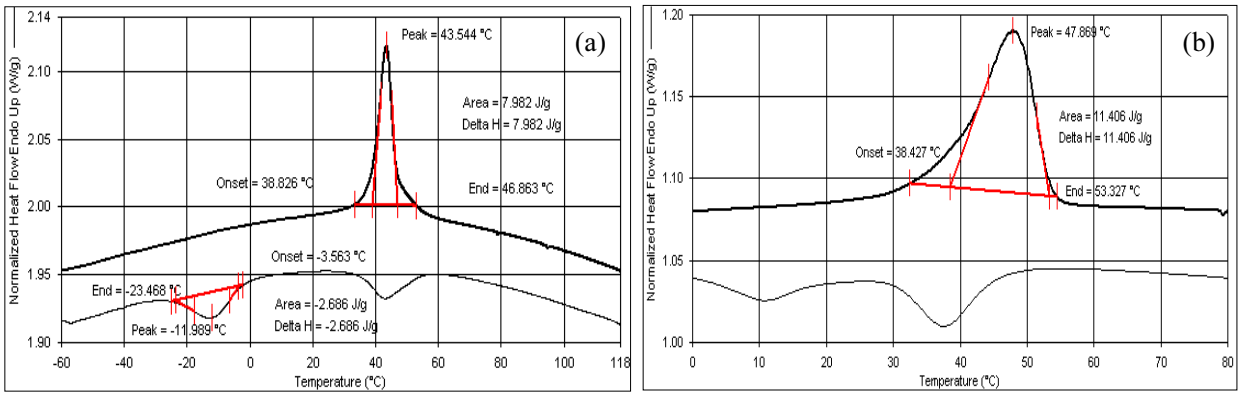

Figure 2: DSC results for porous NiTi: (a) small pore alloy; (b) large pore alloy.

any further processing such as marforming[27] or ausforming. Load from a hydraulic MTS load frame was applied through two compression plates. An extensometer was used to take the strain measurements during testing. A resistance heated chamber was used to elevate the temperature of the test section to 60°C, slightly above the austenite finish temperature for both the small and large pore specimens (refer to Figure 2). The specimens were tested using a cyclic loading-unloading pattern by loading quasi-statically up to a stress and strain level and then unloading to zero stress. For each subsequent cycle, the stress and/or strain were increased with respect to the previous level. The resulting stress-strain response for a typical small pore specimen, tested at a temperature of 60°C is shown in Figure 3a and shows pseudoelastic strain recovery of approximately 1.5% upon unloading. However, full strain recovery is not observed even after heating of the specimen, which is due to plastic strain development in the SMA matrix. The value of the residual plastic strains is approximately 0.9%. The typical stress-strain response for a large pore specimen also tested at 60°C is shown in Figure 3b. The results for the second specimen show pseudoelastic strain recovery of approximately 1.6% and residual strain of 2.8% and are qualitatively similar to the result for the small pore specimen. However, certain distinctions are observed from Figures 3a and 3b. The initial tangent stiffness of the austenite and martensite are different in the two specimens. The stiffness of the austenite in the large pore specimen is approximately twice as large as that of the small pore specimen austenite. This difference in the stiffness may be partially due to incomplete diffusion of the powders in the small pore specimen and the resulting partial adherence of the powder particles. The difference in the pore volume fraction of the two types of specimens also contributes to the difference in the stiffness. Thus, while the maximum reached strain level for the two specimens is similar, the stress levels differ significantly.

There are several possible reasons for the large amount of plastic strain observed during mechanical loading. Initially, since the material has not undergone any thermomechanical loading, the plastic strains develop simultaneously with the transformation strain during martensitic phase transformation. It is a collective result of the accommodation of different martensitic variants during the phase transformation. Due to the misfit between the austenite-martensite interfaces significant distortion is created. In addition, in a polycrystalline SMA different grains transform in a different manner. This causes additional distortion and movement of the grain boundaries. Another source of the plastic strain is the irregular pore shape in the porous SMA. These irregularities create stress concentrations which lead to additional development of plastic strains. These phenomena act in concert and the final result is an observable macroscopic plastic strain. Some other likely reasons for the unrecoverable inelastic strains can be attributed to the fabrication difficulties associated with powder metallurgy techniques, including the presence of other various intermetallic phases due to incomplete diffusion, as described in Section 2.1. These other phases phases embrittle the material, causing the porous material to form microcracks and result in unrecoverable deformation at relatively low strains.

When a large pore specimen is loaded to strain levels beyond 5% it starts to fail by forming microcracks,

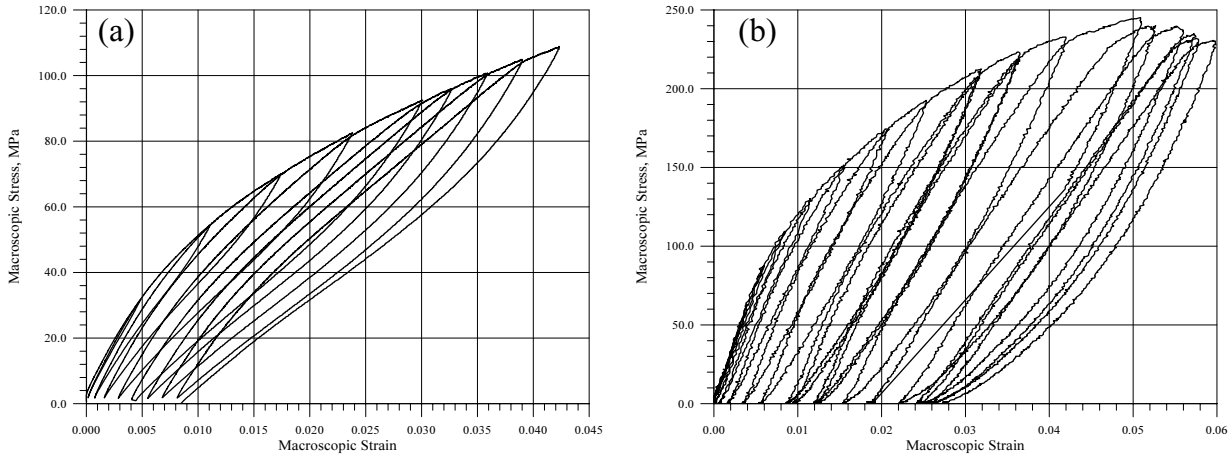

Figure 3: Stress-strain response of porous NiTi tested at 60°C: (a) small pore alloy; (b) large pore alloy.

which was evident by the cracking and popping noises during loading. This failure is identified on the stress-strain curve by the decrease of the stress as the strain is increased (Figure 3b). On the other hand the small pore specimens failed catastrophically, forming large cracks that propagated throughout the entire specimen, causing the specimen to break into multiple fragments.

3. MODELING OF POROUS SMAS

3.1. Micromechanical Model for Porous SMAs

In this section the mechanical behavior of porous NiTi is modeled using micromechanical averaging model developed by Entchev and Lagoudas.[24] The model treats the porous SMA as a composite material with an SMA matrix and pores as second phase. Only the final expressions of the model are presented here, while the details of the derivation of the model can be found in the cited references. The porous SMA composite is characterized by its effective elastic stiffness $\mathbf{L}$, effective tangent stiffness $\mathbf{T}$ and effective stress $\mathbf{\Sigma}$, strain $\mathbf{E}$ and inelastic strain $\mathbf{E}^{in}$. The following expressions for the overall elastic stiffness, tangent stiffness and the evolution of the overall inelastic strain have been derived by Entchev and Lagoudas[24]:

$$\mathbf{L} = c^m \mathbf{L}^m \mathbf{A}^{el,m}, \tag{1}$$

$$\mathbf{T} = c^m \mathbf{T}^m \mathbf{A}^m. \tag{2}$$

$$\dot{\mathbf{E}}^{in} = (\mathbf{I} - (\mathbf{A}^{el,m})^{-1}\mathbf{A}^m) : \dot{\mathbf{E}} + (\mathbf{A}^{el,m})^{-1} : \langle \dot{\boldsymbol{\varepsilon}}^{in,m} + \dot{M}^m : \boldsymbol{\sigma}^m \rangle_m - \dot{\mathbf{M}} : \mathbf{\Sigma}. \tag{3}$$

where $\mathbf{A}^{el,m}$ is the average *elastic* matrix strain concentration factor, $\mathbf{A}^m$ is the average *instantaneous* matrix strain concentration factor; $\mathbf{L}^m$, $\mathbf{M}^m$, $\mathbf{T}^m$ and $\boldsymbol{\varepsilon}^{in,m}$ are the matrix elastic stiffness, elastic compliance, tangent stiffness and transformation strain, respectively. c^m is the volume fraction of the matrix phase, which is given in terms of the porosity c^p by $c^m = 1 - c^p$. The average of the term $\dot{\boldsymbol{\varepsilon}}^{in,m} + \dot{M}^m : \boldsymbol{\sigma}^m$ in the above equation is taken over the matrix phase. Note that the elastic strain concentration factors must me calculated assuming elastic behavior of the phases. The above derived equations can easily be generalized for the case of a composite with any number of phases. The concentration factors $\mathbf{A}^{el,m}$ and $\mathbf{A}^m$ are evaluated using the Mori-Tanaka method and the shape of the pores. A spherical pore shape is used in the numerical calculations in this work.

3.2. Constitutive Model for Fully Dense SMA

The dense SMA matrix constitutive model used in this work is a three-dimensional thermomechanical constitutive model for SMAs which is able to take into account the simultaneous development of transformation

and plastic strains during martensitic phase transformation. The model is an extension of the one-dimensional model presented by Bo and Lagoudas[28–31] to three dimensions.

The constitutive model for the dense SMA matrix is briefly summarized here for the case of isothermal loading. The total strain $\boldsymbol{\varepsilon}^m$ is given by

$$\boldsymbol{\varepsilon}^m = \mathbf{M}^m : \boldsymbol{\sigma}^m + \boldsymbol{\varepsilon}^{t,m} + \boldsymbol{\varepsilon}^{p,m}. \tag{4}$$

The evolution equations for the transformation strain $\boldsymbol{\varepsilon}^{t,m}$ and the plastic strain $\boldsymbol{\varepsilon}^{p,m}$ are given by

$$\dot{\boldsymbol{\varepsilon}}^{t,m} = \boldsymbol{\Lambda}\dot{\xi}, \tag{5}$$

$$\dot{\boldsymbol{\varepsilon}}^{p,m} = \boldsymbol{\Lambda}^p\dot{\zeta}^d, \tag{6}$$

where ξ is the martensitic volume fraction and $\boldsymbol{\Lambda}$ and $\boldsymbol{\Lambda}^p$ are defined as

$$\boldsymbol{\Lambda} = \begin{cases} \frac{3}{2}H^{\mathrm{cur}}\frac{\boldsymbol{\sigma}^{\mathrm{eff},m\prime}}{\bar{\sigma}^{\mathrm{eff},m}} & \dot{\xi} > 0, \\ \frac{\boldsymbol{\varepsilon}^{t,m}_{\max}}{\xi_{\max}} & \dot{\xi} < 0, \end{cases} \tag{7}$$

$$\boldsymbol{\Lambda}^p = \begin{cases} \frac{3}{2}C_1^p \exp\left[-\frac{\zeta^d}{C_2^p}\right]\frac{\boldsymbol{\sigma}^{\mathrm{eff},m\prime}}{\bar{\sigma}^{\mathrm{eff},m}}, & \dot{\xi} > 0, \\ C_1^p \exp\left[-\frac{\zeta^d}{C_2^p}\right]\frac{\boldsymbol{\varepsilon}^{t,m}_{\max}}{\bar{\varepsilon}^t_{\max}}, & \dot{\xi} < 0, \end{cases} \tag{8}$$

The quantity H^{cur} appearing in the above equation is defined to be the *maximum current transformation strain* and is a function of the applied stress. It is a measure of the degree of "detwinning" of the martensitic variants. The quantity ζ^d is the accumulated detwinned martensitic volume fraction and is given by

$$\zeta^d = \int_0^t \frac{H^{\mathrm{cur}}}{H}|\dot{\xi}(\tau)|\mathrm{d}\tau, \tag{9}$$

where H is the limiting value of H^{cur} for large values of the applied stress.

The effective stress $\boldsymbol{\sigma}^{\mathrm{eff},m}$ is defined in terms of the applied stress $\boldsymbol{\sigma}^m$ and the back stress $\boldsymbol{\alpha}^m$ as

$$\boldsymbol{\sigma}^{\mathrm{eff},m} = \boldsymbol{\sigma}^m + \boldsymbol{\alpha}^m. \tag{10}$$

The transformation function Φ is defined as

$$\Phi = \begin{cases} \pi - Y, & \dot{\xi} > 0, \\ -\pi - Y, & \dot{\xi} < 0. \end{cases} \tag{11}$$

In the above equation π is the thermodynamic force conjugate to ξ and is given by

$$\pi = \frac{1}{2}\boldsymbol{\sigma}^m : \Delta\mathbf{M}^m : \boldsymbol{\sigma}^m + \boldsymbol{\sigma}^{\mathrm{eff},m} : \frac{\partial\boldsymbol{\varepsilon}^{t,m}}{\partial\xi} + \eta^m + \rho\Delta s_0(T - M^{0s}) + Y. \tag{12}$$

The back stress $\boldsymbol{\alpha}^m$ and is given by the following polynomial function:

$$\boldsymbol{\alpha}^m = -\frac{\boldsymbol{\varepsilon}^t}{\bar{\varepsilon}^t}\sum_{i=1}^{N^b} D_i^b(H^{\mathrm{cur}}\xi)^{(i)}, \tag{13}$$

where N^b is the degree of the polynomial and D_i^b are the coefficients associated with the back stress. The drag stress η^m is given by the following expression:

$$\eta = -D_1^d\left[-\ln(1-\xi)\right]^{\frac{1}{m_1}} + D_2^d\xi, \tag{14}$$

where D_1^d, D_2^d and m_1 are parameters governing the evolution of the drag stress.

The evolution of the martensitic volume fraction ξ is constrained by the Kuhn–Tucker conditions

$$\begin{aligned} \dot{\xi} \geq 0, \quad \Phi \leq 0, \quad \Phi\dot{\xi} = 0, \\ \dot{\xi} \leq 0, \quad \Phi \leq 0, \quad \Phi\dot{\xi} = 0. \end{aligned} \tag{15}$$

Thus the response of the dense SMA matrix is fully characterized by the system of algebraic and differential equations (4)–(6) which is constrained by equation (15). The constitutive models for the dense and porous SMA have been implemented using the User-Material (UMAT) subroutine capabilities of the finite element package ABAQUS.

3.3. Estimation of the Material Parameters

Using the experimental data presented in Section 2 the material parameters for both types of porous NiTi alloy are estimated in this section. First, the estimation of the parameters for the small pore NiTi alloy is presented. Care must be exercised when taking into account the porosity. Initially, the material parameters for a transformation cycle without plastic strains are estimated. To accomplish this, the residual plastic strain after each increment is subtracted from the total strain. Thus, only the elastic/phase transformation response is obtained. The material parameters are estimated for a transformation loop which is the envelope of the experimental results.

To proceed with the estimation of the material properties, it is assumed that the SMA matrix is isotropic with Poisson's ratio $\nu^A = \nu^M = 0.33$. Next, the Young's elastic moduli of austenite and martensite are evaluated by solving the inverse Mori–Tanaka problem for the porous material and using the experimental data. The value of the effective Young's modulus of the porous austenite is measured using the slope at the beginning of the loading and the corresponding value of the Young's modulus for the austenitic matrix is evaluated from the inverse Mori–Tanaka method to be $E^A = 19.7$ GPa. Similarly, the value of the effective Young's modulus of the porous martensite is obtained using the unloading slope of the last loading cycle, which results in $E^M = 19.0$ GPa. The martensitic start temperature M^{0s} is determined from the calorimetric test data, shown in Figure 2. The cooling curve in Figure 2 shows evidence of a dual peak that is indicative of an R-phase. The second peak was used to obtain the value of the martensitic start temperatures $M^{0s} = 269.5$ K.

The experimental stress-strain curves for porous NiTi differ from the stress-strain response for fully dense NiTi alloy. Namely, it is expected that after initial hardening the pseudoelastic stress-strain curve reaches a plateau with subsequent hardening after the phase transformation is complete. However, the stress-strain response shown in Figure 3a reaches a plateau without exhibiting the second hardening. In addition, the value of the recovered transformation strain is smaller than expected for a NiTi alloy. Therefore, this result suggests that the material does not undergo full austenite-to-martensite phase transformation. Thus, the value of the maximum transformation strain cannot be accurately obtained using the available experimental data. To overcome this difficulty, a value of the maximum transformation strain $H = 3\%$ which is typical for NiTi has been used in this work. Then, it follows that the maximum value of the martensitic volume fraction ξ reached during the stress loading is approximately equal to 0.5. The rest of the material parameters include the hardening parameters as well as the parameter describing the temperature influence on the onset of the transformation. These parameters are also obtained from the experimental data, shown in Figure 3. Once the parameters for a single transformation cycle are determined, the parameters connected with the development of the plastic strains are obtained. The experimental data is also utilized in the estimation of these parameters.

The material parameters for the large pore porous NiTi alloys are estimated following the same procedure. Only the data before the occurring of the microcracking (see Figure 3b) is used to estimate the material parameters. The Young's elastic modulus for the austenite and the martensite are estimated to be $E^A = 42.0$ GPa and $E^M = 32.0$ GPa, respectively. The martensitic start temperature M^{0s} is estimated to be equal to 293.0 K.

4. RESULTS AND DISCUSSIONS

The comparison of the compressive stress-strain response for the small pore NiTi alloy simulated by the model with the experimental data is shown in Figure 4. The material properties obtained in the previous section have

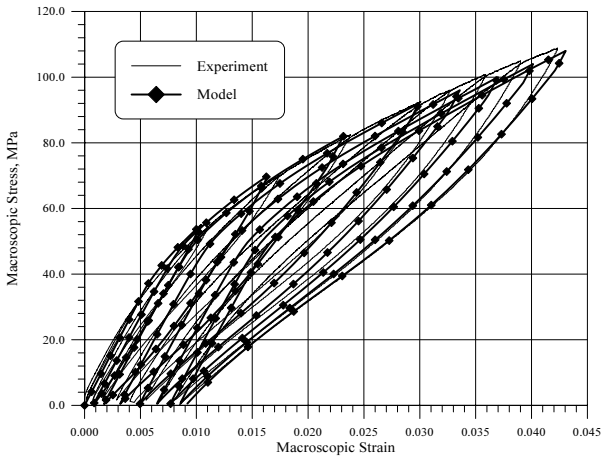

Figure 4. Stress-strain response of a small pore porous NiTi SMA bar — comparison between the experimental results and the model simulation.

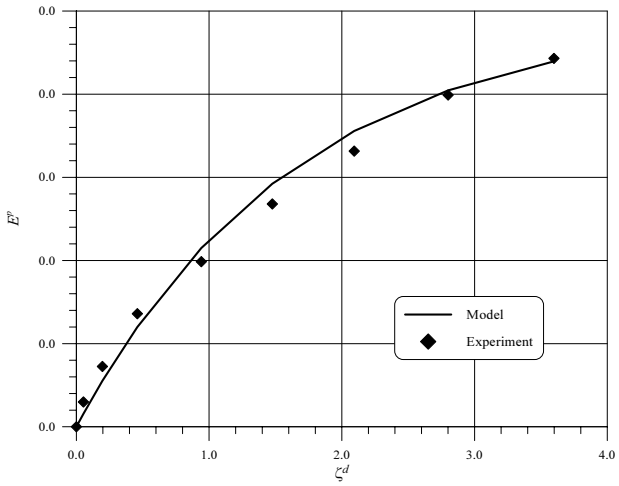

Figure 5. Plastic strain E^p versus accumulated detwinned martensitic volume fraction ζ^d for the small pore porous NiTi.

been used during the numerical calculations. Overall, very good agreement between the results is obtained. Several observations are made from Figure 4. First, the effective Young's moduli for both austenite and martensite are correctly reproduced by the model, since their values have been used for the model calibration. The slope of the stress-strain curve during the transformation is in good agreement with the experimental data. The behavior of the material during minor loops is correctly predicted by the model.

Next, the comparison of the plastic strain predicted by the model with the plastic strain developed during the testing of the material is presented. The evolution of plastic strain in the direction of the loading E^p is presented as a function of the accumulated detwinned martensitic volume fraction ζ^d, which is proportional to the number of loading cycles. The comparison of the model simulation with the experimental data is shown in Figure 5. It can be concluded that by proper calibration of the material parameters the model is capable of correctly simulating the experimental results.

Similar results have been calculated for the large pore porous NiTi alloy. The loading cycles before microcracking were predicted by the model. The comparison of the numerical results with the experimental stress-strain data is shown in Figure 6. It can be seen that the results of the numerical simulations are in good agreement with the experimental data. The plot of the plastic strain versus the accumulated detwinned martensitic volume fraction is shown in Figure 7.

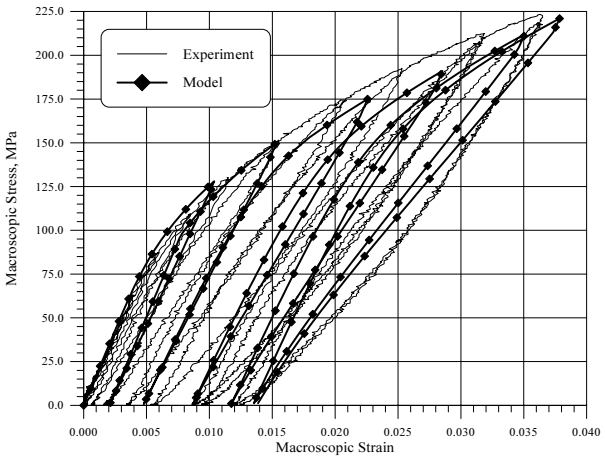

Figure 6. Stress-strain response of a large pore porous NiTi SMA bar — comparison between the experimental results and the model simulation.

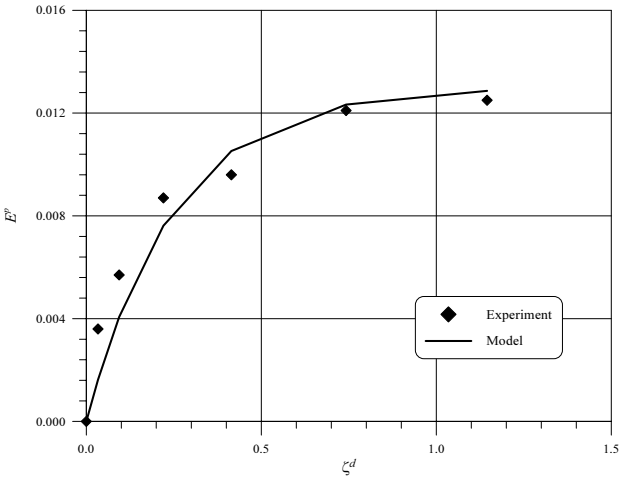

Figure 7. Plastic strain E^p versus accumulated detwinned martensitic volume fraction ζ^d for the large pore porous NiTi.

5. CONCLUSIONS

Porous NiTi alloys with different properties and levels of porosity have been fabricated from elemental Ni and Ti powders using powder metallurgy techniques. The alloys were analyzed and mechanically tested under compressive load. The testing results have shown that the porous NiTi exhibits pseudoelastic behavior. In addition, the development of plastic strain has also been observed.

The behavior of the porous SMAs has been modeled using micromechanical averaging techniques. The behavior of the dense SMA matrix has been accounted for using a thermomechanical constitutive model with internal variables. The model for the SMA matrix accounts not only for the development of transformation strains but also for simultaneous development of plastic strains during phase transformation.

The material parameters for the porous NiTi alloys have been estimated using the experimental data. The mechanical behavior of the porous NiTi under compressive loading has been simulated using the developed model. It has been concluded that the model is capable of simulating the experimental data by calibrating the material parameters.

ACKNOWLEDGMENTS

The authors acknowledge the financial support of the Office of Naval Research Grant No. M00014-99-1-1069 monitored by Dr. Roshdy Barsoum and the support from the Texas Higher Education Coordinating Board TD&T Grant No. 000512-0278-1999.

REFERENCES

1. A. P. Jardine, J. M. Kudva, C. Martin, and K. Appa, "Shape memory alloy Ti-Ni actuators for twist control of smart wing designs," in *SPIE Proceedings of Mathematics and Controls in Smart Structures*, **2717**, pp. 160–165, SPIE, (San Diego, CA), 1996.
2. C. Liang, F. Davidson, L. M. Schetky, and F. K. Straub, "Applications of torsional shape memory alloy actuators for active rotor blade control — opportunities and limitations," in *SPIE Proceedings of Mathematics and Controls in Smart Structures*, **2717**, pp. 91–100, 1996.
3. L. N. Garner, L. J. Wilson, D. C. Lagoudas, and O. K. Rediniotis, "Development of a shape memory alloy actuated biomimetic vehicle," *Smart Materials and Structures* **9**(5), pp. 673–683, 2000.

4. A. Ilyin, M. Dudin, and I. Makarova, "NiTi instruments for TMJ surgeries," in *Superelastic Shape Memory Implants in Medicine*, p. 61, 1995.
5. V. Brailovski and F. Trochu, "Review of shape memory alloys medical applications in Russia," *Bio-Medical of Materials & Engineering* **6**(4), pp. 291–298, 1996.
6. V. E. Gyunter, P. Sysoliatin, and T. Temerkhamor, *Superelastic Shape Memory Implants in Maxillofacial Surgery, Traumatology, Orthopedics, and Neurosurgery*, Tomsk University Publishing House, Tomsk, 1995.
7. K. N. Melton, "General applications of SMA's and smart materials," in *Shape Memory Alloys*, K. Otsuka and C. M. Wayman, eds., ch. 10, pp. 220–239, Cambridge University Press, 1999.
8. I. Ohkata and Y. Suzuki, "The design of shape memory alloy actuators and their applications," in *Shape Memory Alloys*, K. Otsuka and C. M. Wayman, eds., ch. 11, pp. 240–266, Cambridge University Press, 1999.
9. S. Miyazaki, "Medical and dental applications of shape memory alloys," in *Shape Memory Alloys*, K. Otsuka and C. M. Wayman, eds., ch. 12, pp. 267–281, Cambridge University Press, 1999.
10. S. A. Shabalovskaya, V. I. Itin, and V. E. Gyunter, "Porous Ni-Ti — a new material for implants and prostheses," in *Proceedings of the First International Conference on Shape Memory and Superelastic Technologies*, pp. 7–12, SMST International Committee, 1994.
11. R. A. Ayers, S. J. Simske, T. A. Bateman, A. Petkus, R. L. C. Sachdeva, and V. E. Gyunter, "Effects of Nitinol implant porosity on cranial bone ingrowth and apposition after 6 weeks," *J. Biomed. Mater. Res.* **45**(1), pp. 42–47, 1999.
12. S. J. Simske, R. A. Ayers, and T. A. Bateman, "Porous materials for bone engineering," in *Porous Materials for Tissue Engineering*, D.-M. Liu and V. Dixit, eds., *Materials Science Forum* **250**, pp. 151–182, Transtech, 1997.
13. D. C. Lagoudas, P. B. Entchev, M. A. Qidwai, and V. G. DeGiorgi, "Micromechanics of porous shape memory alloys," in *Proceedings of 2000 ASME International Mechanical Engineering Congress & Exposition*, J. Redmont and J. Main, eds., pp. 41–50, 2000.
14. J. C. Hey and A. P. Jardine, "Shape memory TiNi synthesis from elemental powders," *Material Science and Engineering A* **188**(1-2), pp. 291–300, 1994.
15. H. C. Yi and J. J. Moore, "The combustion synthesis of Ni-Ti shape memory alloys," *JOM* **42**, pp. 31–35, 1990.
16. N. V. Goncharuk, I. F. Martynova, O. R. Naidenova, V. V. Skorokhod, S. M. Solonin, and G. R. Fridman, "Superelasticity and shape memory of sintered porous titanium nickelide," *Poroshk. Metall.* **4**, pp. 56–60, 1992.
17. V. I. Itin, V. E. Gyunter, S. A. Shabalovskaya, and R. L. C. Sachdeva, "Mechanical properties and shape memory of porous Nitinol," *Materials Characterization* **32**, pp. 179–187, 1994.
18. O. M. Shevchenko, G. V. Gavrilyuk, V. V. Kokorin, and V. A. Chernenko, "Obtaining Fe-Ni-Co-Ti alloys having a thermoelastic martensite transformation," *Powder Metallurgy and Metal Ceramics* **36**(1-2), pp. 71–76, 1997.
19. B.-Y. Li, L.-J. Rong, and Y.-Y. Li, "Porous NiTi alloy prepared from elemental powder sintering," *J. Mater. Res.* **13**, pp. 2847–2851, 1998.
20. E. L. Vandygriff, D. C. Lagoudas, K. Thangaraj, and Y.-C. Chen, "Porous shape memory alloys, Part I: Fabrication and characterization," in *Proceedings of ASC 15th Annual Technical Conference*, 2000.
21. K. Tangaraj, Y.-C. Chen, and K. Salama, "Fabrication of porous NiTi shape memory alloy by elemental powder sintering," in *Proceedings of 2000 ASME International Mechanical Engineering Congress & Exposition*, J. Redmont and J. Main, eds., pp. 59–63, 2000.
22. M. A. Qidwai, P. B. Entchev, D. C. Lagoudas, and V. G. DeGiorgi, "Modeling of the thermomechanical behavior of porous shape memory alloys," *International Journal of Solids and Structures* **38**, pp. 8653–8671, 2001.
23. D. C. Lagoudas, P. B. Entchev, and E. L. Vandygriff, "Fabrication and modeling of porous shape memory alloys," in *Proceedings of ASC 16th Annual Technical Conference*, 2001.
24. P. B. Entchev and D. C. Lagoudas, "Modeling porous shape memory alloys using micromechanical averaging techniques," *Mechanics of Materials* **34**(1), pp. 1–24, 2002.

25. D. C. Lagoudas, Z. Bo, and M. A. Qidwai, "A unified thermodynamic constitutive model for SMA and finite element analysis of active metal matrix composites," *Mechanics of Composite Materials and Structures* **3**, pp. 153–179, 1996.
26. D. C. Lagoudas and E. L. Vandygriff, "Processing and characterization of NiTi porous SMA by elevated pressure sintering." Submitted to: *Journal of Intelligent Material Systems and Structures*, January 2002.
27. D. Wurzel, "Marforming and tempering of binary Ni-Ti alloys including precipitation effects," *Material Science and Engineering A* **273–275**, pp. 634–638, 1999.
28. Z. Bo and D. C. Lagoudas, "Thermomechanical modeling of polycrystalline SMAs under cyclic loading, Part I: Theoretical derivations," *International Journal of Engineering Science* **37**, pp. 1089–1140, 1999.
29. Z. Bo and D. C. Lagoudas, "Thermomechanical modeling of polycrystalline SMAs under cyclic loading, Part III: Evolution of plastic strains and two-way memory effect," *International Journal of Engineering Science* **37**, pp. 1141–1173, 1999.
30. Z. Bo and D. C. Lagoudas, "Thermomechanical modeling of polycrystalline SMAs under cyclic loading, Part IV: Modeling of minor hysteresis loops," *International Journal of Engineering Science* **37**, pp. 1174–1204, 1999.
31. D. C. Lagoudas and Z. Bo, "Thermomechanical modeling of polycrystalline SMAs under cyclic loading, Part II: Material characterization and experimental results for a stable transformation cycle," *International Journal of Engineering Science* **37**, pp. 1205–1249, 1999.